Predetermined control of turbulent boundary layer with a piezoelectric oscillator*

Xiao-Bo Zheng(郑小波)[1], Nan Jiang(姜楠)[1,2,†], and Hao Zhang(张浩)[1]

[1] *Department of Mechanics, Tianjin University, Tianjin* 300072, *China*
[2] *Tianjin Key Laboratory of Modern Engineering Mechanics, Tianjin* 300072, *China*

(Received 3 May 2015; revised manuscript received 10 August 2015; published online 30 November 2015)

With a piezoelectric (PZT) oscillator, the predetermined controls of the turbulent boundary layer (TBL) are effective in reducing the drag force. The stream-wise velocities in the TBL are accurately measured downstream of the oscillator driven by an adjustable power source. The mean velocity profiles in the inner and outer scales are reported and the skin friction stresses with different voltage parameters are compared. Reduction of integral spatial scales in the inner region below y^+ of 30 suggests that the oscillator at work breaks up the near-wall stream-wise vortices responsible for high skin friction. For the TBL at Re_θ of 2183, the controls with a frequency of 160 Hz are superior among our experiments and a relative drag reduction rate of 26.83% is exciting. Wavelet analyses provide a reason why the controls with this special frequency perform best.

Keywords: turbulent boundary layer, predetermined control, drag reduction, piezoelectric oscillator

PACS: 47.85.lb, 47.85.ld, 47.27.nb, 47.27.De **DOI:** 10.1088/1674-1056/25/1/014703

1. Introduction

High skin friction generated by turbulent boundary layer (TBL) flow makes the drag reduction control a significant topic not only in fluid mechanics but also in other engineering areas. Coherent structure, i.e., multi-scale quasi-order spatiotemporal structure in a self-sustaining mechanism, plays a key role in the dynamics of the TBL.[1–6] Among them, stream-wise vortices near the wall are responsible for high skin friction regions underneath the TBL,[7,8] as shown in Fig. 1. From the perspective of control, a method that can manipulate stream-wise vortices and impede the self-generating process is beneficial to the purpose of skin-friction drag reduction.[9–12]

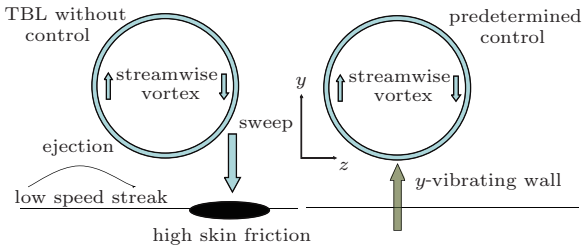


Fig. 1. Schematic of predetermined control for drag reduction.

Compared with passive methods,[13–18] the active control has a wide adaptability to complex flows and can amplify the control effectiveness with a small auxiliary energy input.[19,20] For the actual implementation, a predetermined method is more feasible than interactive control.[21–23] Because of its low power consumption, fast response and low cost, piezoelectric (PZT) material driving an oscillator with a forcing alternating voltage (AV) can be utilized as an actuator of predetermined control.[24]

In this paper, a rectangular PZT oscillator is applied. We elaborate the oscillator used and examine the effect of the varied AV amplitude and frequency. To characterize the control performance, the statistical magnitudes of the TBL, such as mean stream-wise velocities and skin friction stress, are reported. The reduction of integral spatial scale in the inner region of the TBL reflects the control influence on the stream-wise vortices near the wall. Wavelet analysis reveals on what scale these structures are and under what AV frequency the control can achieve a better drag reduction.

2. Experiment setup

2.1. Basic TBL flow field

The experiments were conducted in an annular return wind tunnel. The TBL flow was developing along one side of a flat acrylic glass plate mounted vertically in the wind tunnel. Following the right-hand rule, the space coordinate system $Oxyz$ is set with O as the origin at the leading edge of the plate, x as the stream-wise direction, y as the wall-normal direction, and z as the span-wise direction as shown in Fig. 2(a). By adjusting the pitch angle of the plate, a nearly zero-pressure-gradient in the x direction was achieved. A piece of twisted-pair wire was fixed spanwisely at $x = 8$ cm, and 4 pieces of No. 240 sandpaper were attached following the wire until $x = 53$ cm. These measures accelerated the transition of the

*Project supported by the National Natural Science Foundation of China (Grant Nos. 11332006, 11272233, and 11411130150) and the National Basic Research Program of China (Grant Nos. 2012CB720101 and 2012CB720103).

†Corresponding author. E-mail: nanj@tju.edu.cn

© 2016 Chinese Physical Society and IOP Publishing Ltd

boundary layer and made us achieve the fully developed TBL flow at about $x = 1000$ mm where the end of the control mechanism was and the measurements were conducted as shown in Fig. 2(b).[25]

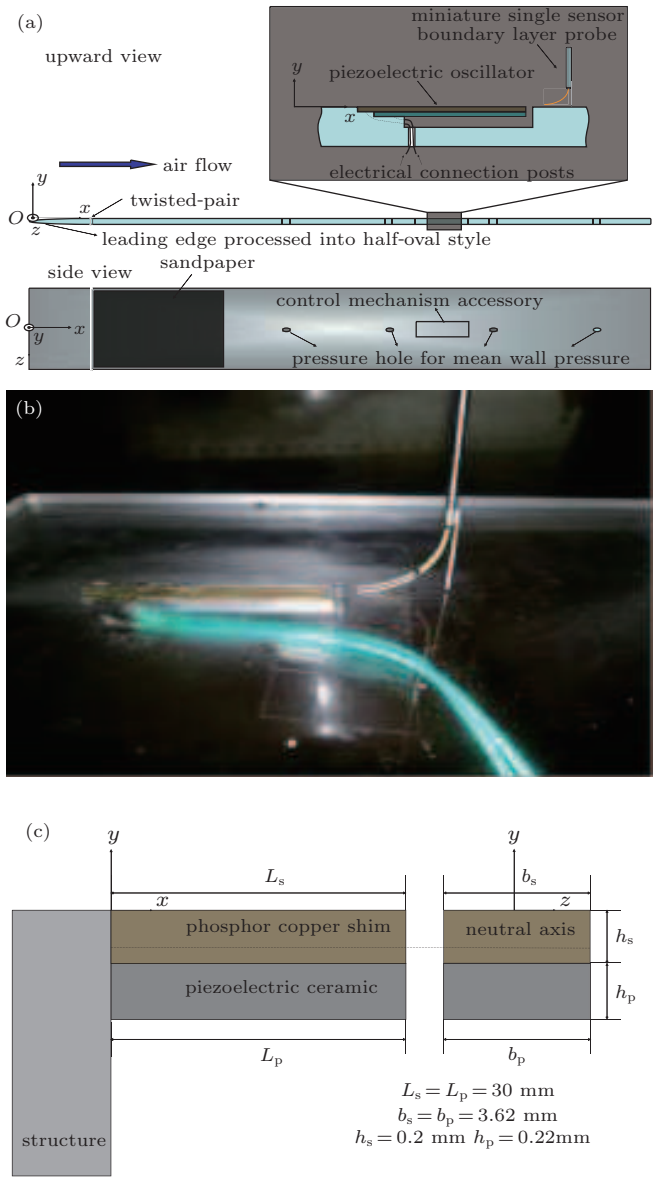


Fig. 2. (a) Schematic of experiment set-up, (b) picture of PZT oscillator and miniature velocity probe, and (c) Euler–Bernoulli beam model of PZT oscillator.

2.2. PZT oscillator

The control mechanism consisted of a cavity with the sizes of 32 mm × 5 mm × 5 mm and a PZT oscillator pasted firmly. The oscillator upper surface was kept flush with the flat plate. The effective length, total thickness, and the width of the oscillator were 30 mm, 0.42 mm, and 3.62 mm. The length and width were designed according to the size of the near-wall stream-wise vortex, a span-wise scale of $O(100\nu/u_\tau)$, and a stream-wise scale of $O(\delta)$ (both defined later). This unimorph configuration consisted of a piece of 220-μm-thick PZT-5H material and a 200-μm-thick phosphor-copper shim. The thickness of epoxy bond was negligible. To excite the PZT oscillator, we used a power source of YuanFang-GK10005 that supplies AV with adjustable frequency and amplitude in a wide range.

The PZT oscillator was modeled as a cantilever beam[26] as shown in Fig. 2(c). When a voltage was applied between its upper and lower surfaces, the beam bent in the x–y plane. The oscillator changed the wall boundary conditions and introduced interference into the TBL. The assumption of perfect bonding implied that the strain was continuous at the bond interface, and a linear strain distribution in the y direction was adopted.

According to the basic geometrical information and material properties of the PZT oscillator (Table 1), we analyze the static deformation and the dynamic vibration by using the Euler–Bernoulli beam theory. For an incompressible air flow, the aerodynamic pressure loading on the oscillator is negligible at low Mach numbers.

Table 1. Details of PZT oscillator materials.

Quantity	Value
PZT density ρ_p/kg·m^{-3}	7.45×10^3
Shim density ρ_s/kg·m^{-3}	8.89×10^3
PZT elastic modulus E_p/N·m^{-2}	7.69×10^{10}
Shim elastic modulus E_s/N·m^{-2}	11.3×10^{10}
PZT strain constant d_{31}/m·V^{-1}	-186×10^{-12}

The first-order natural frequency f_1 is 254 Hz and the direct voltage (DV) gain coefficient H_0, i.e., the tip displacement of the PZT oscillator actuated by a voltage of 1 V, is 0.0014 mm/V. These two parameters are both important for the second-order frequency response model which has been verified experimentally.[27] The model of AV gain coefficient $H(f)$ can be expressed as

$$H(f) = H_0 / \left[1 - (f/f_n)^2 + \mathrm{j}(2\xi f/f_n)\right], \qquad (1)$$

where f_n is the n-th-order natural frequency, and ξ is the damping ratio and can be neglected for its small magnitude. Figure 3 shows the curve of the frequency response function. We set the AV control frequency f_c to be below f_1 to ensure the zero phase difference and appropriate gain. The tip displacement of the PZT oscillator is proportional to the applied voltage amplitude. Because of the voltage limit of the PZT material used, we supply voltage amplitudes V_c of no larger than 100 V for safety. The tip amplitudes A_t of the PZT oscillator in different working conditions are shown in Table 2.

Under most control conditions, the interference introduced by the PZT oscillator belongs to the category of the Hydrodynamic smooth, because their amplitudes are less than 7 wall units (1 wall unit = ν/u_τ) (~ 0.257 mm). Although the amplitudes are a little bigger than the critical condition of the Hydrodynamic smooth when f_c is set to be 240 Hz, the typical layered structure of the TBL is not altered, owing to the small size of the PZT oscillator compared with the whole flow field.

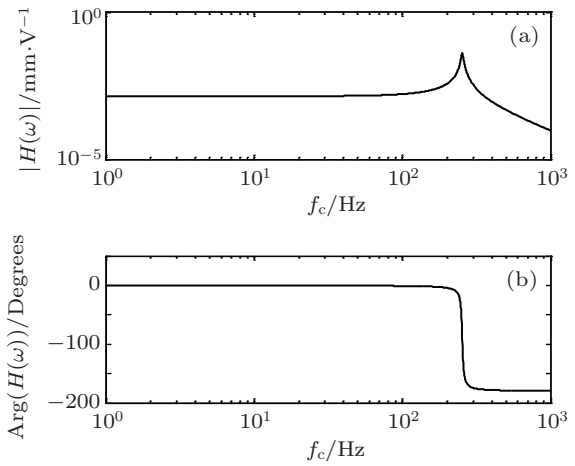


Fig. 3. Frequency responses of PZT oscillator. (a) Amplitude–frequency curve, (b) phase–frequency curve.

Table 2. Drag reduction effect at $x = 1002$ mm.

V_c/V, f_c/Hz	A_t/mm	τ_w/(N/m^2)	$\Delta\tau_w/\tau_w^N$	u_τ/(m/s)
No control	0	0.2408	0	0.4317
20, 80	0.031	0.2421	0.54%	0.4329
20, 160	0.046	0.2416	0.33%	0.4324
20, 240	0.261	0.2488	3.32%	0.4388
60, 80	0.093	0.2348	–2.49%	0.4263
60, 160	0.139	0.2066	–14.20%	0.3999
60, 240	0.784	0.2400	–0.33%	0.4310
100, 80	0.155	0.2037	–15.41%	0.3971
100, 160	0.232	0.1762	–26.83%	0.3693
100, 240	1.306	0.2290	–4.90%	0.4210

2.3. Velocity measurement

At $x = 1002$ mm, i.e., 2 mm downstream the end of the control mechanism, the stream-wise velocity components u in the TBL were accurately measured by the constant temperature anemometry of IFA-300 with a miniature boundary layer probe TSI-1621A-T1.5. The hot wire of this probe is made of tungsten (platinum coated) cylinder with a sensitive length of 1.25 mm and diameter of 4 μm. This probe was specially prepared for velocity measurement, which was located very close to the wall.[28,29] Before measurement, mean-flow calibration was employed twice and the error was 0.087% based on the fourth-order polynomial curve fitting. We set the sampling rate and low pass cut off frequency to be 100 kHz and 50 kHz, respectively. Time sequences of the stream-wise velocity signals at different wall-normal locations were finally achieved and each sequence consisted of 2^{22} moments in about 42 s.

3. Result and analysis

3.1. Mean velocity and skin friction

The free stream velocity U_∞ is 9.0 m/s and the TBL nominal thickness δ is 39.8 mm. Based on U_∞ and the momentum thickness θ, the Reynolds number Re_θ is 2183. The outer scale mean velocity profile (scaled with δ and U_∞) is linear in the viscous sub-layer[30,31] as indicated in Fig. 4(a). The profile slope is related to skin friction stress τ_w, because

$$\tau_w = \rho\nu\partial U/\partial y, \tag{2}$$

where air flow density ρ is 1.205 kg/m^3 and kinematic viscosity coefficient ν is 1.5×10^{-5} m^2/s.[32–34] The skin friction velocity u_τ can be obtained according to

$$\tau_w = \rho u_\tau^2. \tag{3}$$

Table 2 shows the values of relative drag reduction rate $\Delta\tau_w/\tau_w^N$ under different values of V_c and f_c, and τ_w^N is the skin friction stress of the TBL without control.

Figure 4(b) shows the mean velocity profiles in inner scale units $y^+ = yu_\tau/\nu$ and $U^+ = U/u_\tau$. According to the log law $U^+ = \kappa^{-1}\ln y^+ + B$, B is related to u_τ as the following differential expression:

$$\mathrm{d}u_\tau/u_\tau = -\mathrm{d}B/\left(U^+ + 1/\kappa\right), \tag{4}$$

where the Karman constant κ is 0.41. Because $\mathrm{d}\tau_w/\tau_w^N$ is twice the value of $\mathrm{d}u_\tau/u_\tau$, $\mathrm{d}B$ becomes a visual measure of control effects in the view of whole TBL. The most beneficial effect of 160 Hz AV is obvious among the control strategies. With f_c kept constant, the drag reduction effect is positively correlated with V_c.

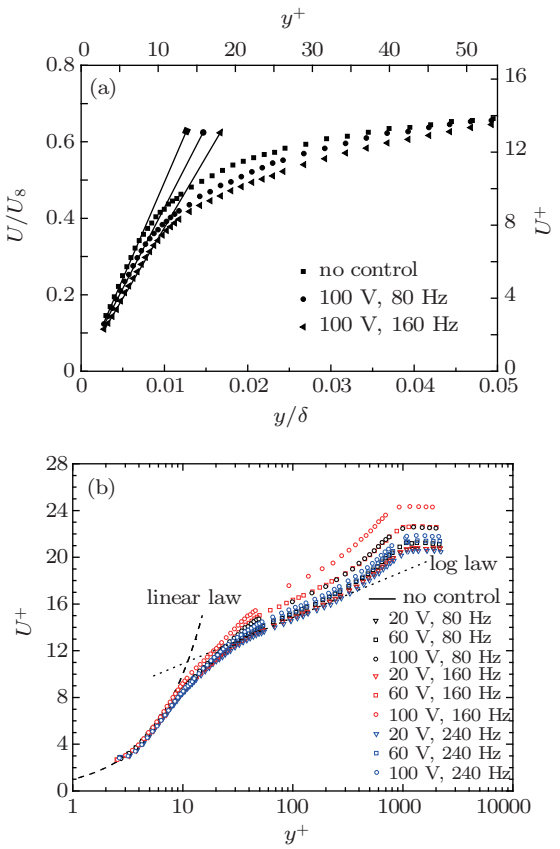


Fig. 4. Mean velocity profiles of different control conditions in (a) outer and (b) inner scale units.

3.2. Integral spatial scale

The integral spatial scale L reflects the spatial dimension of a turbulent structure in large scale with the same order of mean motion,[25] and is achieved by the auto-correlation analysis and Taylor's frozen hypothesis as

$$L\left(y^{+}\right)=U\left(y^{+}\right)\times\int_{0}^{\infty}f\left(\tau\right)\mathrm{d}\tau\big|_{y^{+}}\,, \tag{5}$$

where $f(\tau)=\overline{u'(t+\tau)u'(t)}/\overline{u'^{2}(t)}$ is the auto-correlation coefficient of longitudinal fluctuating velocity temporal sequence $u'(t)$. As Fig. 5 shows, in the outer portion of the TBL, L keeps the same order as δ and curves of different control conditions overlap well. However, in the inner region of $y^{+}<30$, it is obvious that L with control is smaller than that without control and L is the smallest when 100 V and 160 Hz AV are both applied. Coupled with the drag reduction effect, it suggests that the PZT oscillator at work breaks up the stream-wise vortices near the wall, which leads to the reduction of high skin friction.

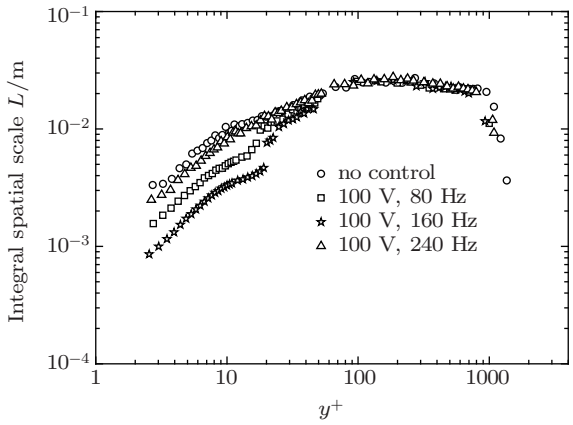


Fig. 5. Profiles of integral special scale L.

3.3. Wavelet analysis

In order to detect the most energetic coherent components of TBL flow and reveal the control mechanism, Mallat pyramidal algorithm of the orthonormal discrete wavelet transform is accomplished with db5 wavelet.[35,36] The wavelet scale index n is linear with respect to logarithmic characteristic frequency f_n^{W}, as Fig. 6(a) shows. The curve slope slightly differs from the dyadic property theoretical value of -1. This deviation is caused by the selection of wavelet basis. The intercept is related to the signal sampling frequency. According to the linear logarithmic relationship, the control frequencies of 80, 160, and 240 Hz are corresponding to varied discrete scale n values of 10, 9, and 8 in the multi-scale system of near-wall turbulence.

The values of single-reconstructed velocity fluctuation $u'_{\mathrm{r}}(n,t)$ without control are attained firstly at different values of wall-normal location y^{+}. Then the energy distribution $\overline{u'^{2}_{\mathrm{r}}}(n,y^{+})$ in dB is shown by Fig. 6(b). A peak at $(n=9,y^{+}=14)$ is obvious and it corresponds to the stream-wise vortex in the buffer layer that is located in a frequency band near the frequency f_9^{W} of about 147 Hz. These structures contain the most fluctuating energy in the near-wall multi-scale turbulence.[37] It is the reason why the controls with a frequency of 160 Hz located in this special frequency band perform best for drag reduction in our experiments.

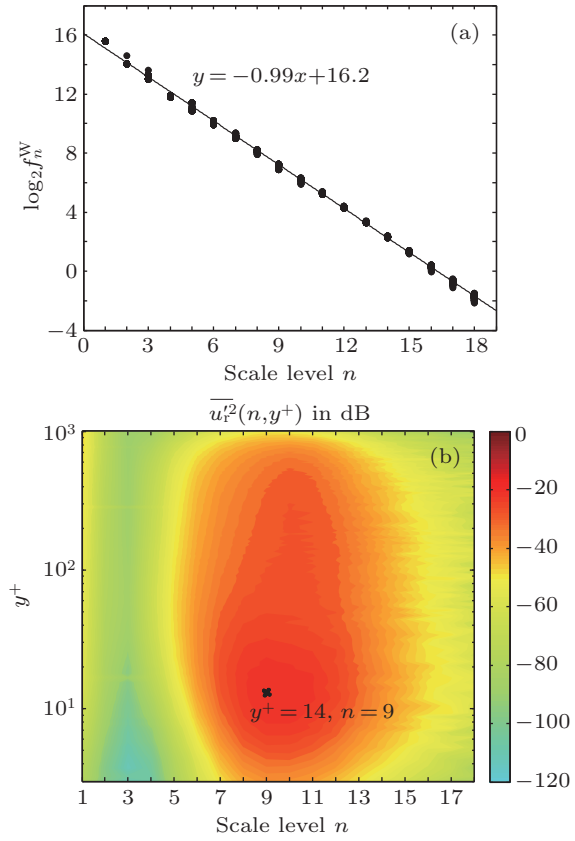


Fig. 6. (a) Relationship between n and f_n^{W}, (b) distribution of $\overline{u'^{2}_{\mathrm{r}}}$ in the plane (n,y^{+}) without control.

4. Conclusions

The PZT oscillator controls of the TBL are effective in reducing the drag force, and the most relative drag reduction rate of 26.83% is noticeable. When the control frequency is fixed, the drag reduction effect is positively correlated with the tip amplitude of PZT oscillator which is proportional to the AV amplitude. The controls are superior when AV frequencies are set to be near the frequency corresponding to the scale of the near-wall coherent structure containing the most energy. Reduction of integral spatial scale in the inner region of $y^{+}<30$ suggests that the PZT oscillator at work breaks up the near-wall stream-wise vortices responsible for high skin friction. Because of the high electrical impedance of PZT oscillator under AV driving, the power consumptions of different control conditions are all less than 0.1 watt measured by a power meter built-in the power supply. In this light, the drag reduction performances of our control strategies are exciting.

References

[1] Robinson S K 1991 *Annu. Rev. Fluid Mech.* **23** 601
[2] Wang W, Guan X L and Jiang N 2014 *Chin. Phys. B* **23** 104703
[3] Wang L and Lu X Y 2011 *Chin. Phys. Lett.* **28** 034703
[4] Zheng X B and Jiang N 2015 *Acta Mech. Sin.* **31** 16
[5] Hu H B, Du P, Huang S H and Wang Y 2013 *Chin. Phys. B* **22** 074703
[6] Tang Z Q and Jiang N 2011 *Chin. Phys. Lett.* **28** 054702
[7] Kim J 2011 *Philos. Trans. R. Soc. A* **369** 1396
[8] Kravchenko A G, Choi H and Moin P 1993 *Phys. Fluids A* **5** 3307
[9] Duguet Y, Schlatter P, Henningson D S and Eckhardt B 2012 *Phys. Rev. Lett.* **108** 044501
[10] Lang S S, Geng X G and Zang D Y 2014 *Acta Phys. Sin.* **63** 084704 (in Chinese)
[11] Duriez T, Aider J L and Wesfreid J E 2009 *Phys. Rev. Lett.* **103** 144502
[12] Wu W T, Hong Y J and Fan B C 2014 *Acta Phys. Sin.* **63** 054702 (in Chinese)
[13] Bechert D W and Bartenwerfer M 1989 *J. Fluid Mech.* **206** 105
[14] Dubief Y, White C M, Terrapon V E, Shaqfeh E S G, Moin P and Lele S K 2004 *J. Fluid Mech.* **514** 271
[15] Wang B, Wang J D and Chen D R 2014 *Acta Phys. Sin.* **63** 074702 (in Chinese)
[16] Min T and Kim J 2004 *Phys. Fluids* **16** L55
[17] van den Berg T H, van Gils D P M, Lathrop D P and Lohse D 2007 *Phys. Rev. Lett.* **98** 084501
[18] Gu Y Q, Mou J G, Dai D S, Zheng S H, Jiang L F, Wu D H, Ren Y and Liu F Q 2015 *Acta Phys. Sin.* **64** 024701 (in Chinese)
[19] Rathnasingham R and Breuer K S 2003 *J. Fluid Mech.* **495** 209
[20] Kim J 2003 *Phys. Fluids* **15** 1093
[21] Deng B Q and Xu C X 2012 *J. Fluid Mech.* **710** 234
[22] Cattafesta L N and Sheplak M 2011 *Annu. Rev. Fluid Mech.* **43** 247
[23] Lee C, Hong G, Ha Q P and Mallinson S G 2003 *Sens. Actuators A* **108** 168
[24] Crawley E F and de Luis J 1987 *AIAA J.* **25** 1373
[25] Zheng X B and Jiang N 2015 *Chin. Phys. B* **24** 064702
[26] Söderkvist J 1991 *J. Acoust. Soc. Am.* **90** 686
[27] Cattafesta L N, Garg S and Shukla D 2001 *AIAA J.* **39** 1562
[28] Hutchins N, Nickels T B, Marusic I and Chong M S 2009 *J. Fluid Mech.* **635** 103
[29] Ligrani P M and Bradshaw P 1987 *Exp. Fluids* **5** 407
[30] Kim J, Moin P and Moser R 1987 *J. Fluid Mech.* **177** 133
[31] DeGraaff D B and Eaton J K 2000 *J. Fluid Mech.* **422** 319
[32] Stefes B and Fernholz H H 2004 *Eur. J. Mech. B* **23** 303
[33] Patel V C and Head M R 1969 *J. Fluid Mech.* **38** 181
[34] Xin Y B, Xia K Q and Tong P 1996 *Phys. Rev. Lett.* **77** 1266
[35] Camussi R and Guj G 1997 *J. Fluid Mech.* **348** 177
[36] Farge M 1992 *Annu. Rev. Fluid Mech.* **24** 395
[37] Jiménez J 2012 *Annu. Rev. Fluid Mech.* **44** 27